Spinal Cord (2017) 55, 411–418

www.nature.com/sc

ORIGINAL ARTICLE

The preparation of rat's acellular spinal cord scaffold and co-culture with rat's spinal cord neuron *in vitro*

D-X Ban, Y Liu, T-W Cao, S-j Gao and S-Q Feng

Study design: The rat's acellular spinal cord scaffold (ASCS) and spinal cord neurons were prepared *in vitro* to explore their biocompatibility.
Objectives: The preparation of ASCS and co-culture with neuron may lay a foundation for clinical treatment of spinal cord injury (SCI).
Setting: Tianjin Medical University General Hospital, China
Methods: ASCS was prepared by chemical extraction method. Hematoxylin and eosin (H&E), myelin staining and scanning electron microscope were used to observe the surface structure of ASCS. Spinal cord neurons of rat were separated *in vitro*, and then co-cultured with prepared ASCS *in virto*.
Results: The prepared ASCS showed mesh structure with small holes of different sizes. H&E staining showed that cell components were all removed. The ASCS possessed fine three-dimensional network porous structure. DNA components were not found in the ASCS by DNA agarose gel electrophoresis. The cultured cells express neuron-specific enolase (NSE) antigen with long axons. H&E staining showed that the neurons adhered to the pore structures of ASCS, and the cell growth was fine. The survival rate of co-cultured cells was ($97.53 \pm 1.52\%$) by MTT detection. Immunohistochemical staining showed that neurons on the scaffold expressed NSE and NeuN antigen. Cells were arranged closely, and the channel structures of ASCS were fully filled with neurons. The cells accumulated in the channel and grew well in good state.
Conclusion: The structure of ASCS remained intact, and the neurons were closely arranged in the scaffolds. These results may lay a solid foundation for clinical treatment of SCI when considering glial scar replacement by biomaterials.
Spinal Cord (2017) **55,** 411–418; doi:10.1038/sc.2016.144; published online 25 October 2016

INTRODUCTION

The incidence of spinal cord injury (SCI) has been gradually increasing year by year, and the treatment has always troubled the medical field all the time. Through the study on the pathogenesis of SCI, pathological and physiological processes of SCI on cellular and molecular levels have already been comprehensively understood. However, the overall prognosis of patients after SCI and the efficacy has not reached the essential breakthrough.[1] Effective treatment of SCI should include the reestablishment of the tissue structure, functional axonal regeneration and removal of local glial scar with the assistance and cooperation of multiple disciplines.[2] Nowadays, polymer materials and three-dimensional (3D) printing technology have been considered to be applied for the treatment of SCI. The application of scaffold materials and simulated 3D structure of autologous spinal cord greatly increased the efficacy of treatment after SCI.[3] However, there is a great difference between scaffold materials and normal human spinal cord in physical and chemical properties. Although the synthetic scaffold materials have the same or similar structure as the receptor spinal cord, there will be a strong immune response after implantation *in vivo*.[4,5] It has been reported that the rejection response, after scaffold implantation, is mainly caused by the scaffold remnants of cellular components and nerve myelin. Extracellular matrix (ECM) components for the immune response are very weak among the same species.[6] Therefore, how to repair the local negative micro-environment after SCI, effectively reduce the scaffold transplantation immune rejection and promote the regeneration of injured nerve have become the focus for the treatment after SCI.[7–9]

SCI causes the damage of internal homeostasis of the spinal cord, resulting in the primary and secondary injury. Primary injury belongs to physical injury (such as tear, contuse, crush and so on) to the spinal cord tissue, which will lead to injury of cells and axons and rupture of blood vessels and so on. Secondary injury belongs to the further development of primary injury, which includes the change of local ion concentration, reduction in the spinal cord blood flow, blood–brain barrier damage, free radical generation and release of the cytotoxicity neurotransmitter and so on.[10–12] Primary and secondary injuries ultimately lead to nerve impulse conduction block. Microglia and astrocytes excessively accumulate and proliferate to form the glial scar.[13–15] The scar will also be uptaken by monocyte macrophage phagocytosis and finally form the cavity. The nerve cells in the glial scar area will finally be curbed and become permanent barriers to impede axonal regeneration.[16] In early stage after SCI, astrogliosis has a protective effect on the neuronal survival and regeneration.[17] However, mature astrocytes and microglia will secrete inhibitory factors (such as proteoglycan, nitric oxide and so on) and form biological glial barrier, which will finally impede nerve regeneration. Excessive proliferation of glial cells and glial scar formation result in

Department of Orthopedics, Tianjin Medical University General Hospital, Tianjin, China
Correspondence: Dr S-Q Feng, Department of Orthopedics, Tianjin Medical University General Hospital, Tianjin Heping District Anshan Road 154, Tianjin 300052, China.
E-mail: fengsq321@sina.com
Received 17 June 2016; revised 30 August 2016; accepted 14 September 2016; published online 25 October 2016

mechanical disorders and affect the axonal regeneration, extension and fusion. Glial scar may form the micro-blood vessel cover to compress blood vessel and reduce the local spinal cord blood supply.[9,18–20] Therefore, reduction of the negative effect of glial scar on nerve regeneration has become the hot point for the treatment of SCI. Biological engineering scaffold implantation is the most effective way to achieve this goal. Tissue engineering scaffold implantation can serve as support matrix for seed cells to grow and isolate or reduce glial scar invasion, to promote and guide regenerated axons to pass through regional transplanted area.[21–24] In the early days, tissue engineering scaffold has been applied for the repair of severe disease and has achieved excellent experimental and clinical curative effect, such as skin and cartilage grafts application.[25–28]

Currently, biodegradable natural or synthetic polymer biomaterials are always used in spinal cord tissue engineering scaffold.[29] Natural biodegradable polymers such as collagen, gelatin, chitosan and so on have good biocompatibility. Their degradation products are not inclined to generate local inflammatory reaction, but their poor biomechanical property made them unable to build a 3D structure, which leads to poor application value. Degradable synthetic polymer materials mainly contain polylactide series of materials. Polylactic acid, polyglycolic acid and their copolymers were used most widely. Their degradation speed and biomechanical strength are acceptable and plastic. They also can construct a 3D scaffold with high porosity. However, under the current technical conditions, it is difficult to truly imitate the complex biological spinal cord 3D space structure.[30]

The most suitable scaffold for SCI should have the following characteristics: the 3D structure for tissue regeneration, regulation function of cellular physiology and immune protection. Acellular spinal cord scaffold (ASCS) is a kind of bionic natural 3D tubular scaffold material, which has fundamental differences and inherent superiority when compared with the traditional biological degradation material graft.

ASCS has its own advantages when compared with other materials, such as easy to get and store, allele and anatomical transplantation, minimized adverse effects on recipients, simple manufacture technology an so on.[31] Therefore, ASCS has become a hot research topic in recent years. In addition to that, vascular network is also an important challenging element for tissue reconstruction. By using a natural body organ, cells were removed with detergent or ion solution; microarchitecture and vascular network can be obtained with these non-cell natural scaffolds as tissue regeneration template.[32]

On the basis of the decellularization, re-endothelialization and autologous cell scaffold, the whole organ was successfully made, such as the heart, lung, kidney and liver. The combined decellularization/re-endothelialization method provides two main advantages. First, the removal of primary cells may reduce the immune response. Second, the real microarchitecture and geometric arrangement can be retained, real microarchitecture can be obtained, which cannot be achieved by using current manufacturing techniques.[33,34]

For SCI, the scar area can be replaced by ASCS; this scaffold retains the microarchitecture of spinal cord, which will guide the regenerated axons to grow. Decellularization removes all the cells in the scaffold. However, neuron was needed to reconstruct the synaptic connection. In this paper, chemical extraction method was applied to prepare the ASCS, which then co-culture with neuron *in vivo* to explore the survival of neurons and their biocompatibility in order to lay a solid foundation for the treatment of SCI.

MATERIALS AND METHODS

Preparation of acellular spinal cord scaffold

Wistar rat was anesthetized by intraperitoneal injection of pentobarbital sodium and then fixed on the prone position. The hair of the rat on the back was removed after the disinfection. The skin was cut at midline on the back, the paravertebral muscles separated, the backbone exposed, the lamina removed and the spinal cord exposed. The spinal cord around 2–3 cm in the center of T10 segment was taken out. The spinal cord was rinsed in phosphate-buffered saline (PBS) to remove blood and completely thawed after being frozen at − 80 °C for 24 h. The spinal cord was soaked with ddH2O at 4 °C for 6 h, then placed in 0.02% trypsin /0.05% EDTA solution at 37 °C for digestion for 1 h, followed by 3.0% Triton X-100 at room temperature for 3 h, 1.0 M sucrose to wash for 15 min and rinsed by ddH2O three times for 10 min. It was then treated with 4.0% sodium deoxycholate at room temperature for 3 h, 0.1% peracetic acid /4.0% ethanol at room temperature for 2 h, washed with PBS three times(10 mins for each time) and rinsed by ddH2O three times (10 mins for each time). After that, the spinal cord tissue was frozen and dried by freeze-drying machine, and then sterilized with ethylene oxide and placed in a sterile EP tube at − 80 °C.

Morphological observation of ASCS

After the ASCS was prepared, the color, transparency, shape, length, toughness and odor were observed.

DNA extraction from spinal cord scaffold of Wistar rat

The ASCS was completely thawed at room temperature, then put into the 1.5 ml centrifuge tube after washing with normal saline, and then cut into pieces. TES, SDS and protease K were put into the tube and keep the temperature at 56 °C for 6 h. After cooling to the room temperature, the same volume of saturated phenol (UL) was added into the tube, centrifuge at 10 000 r.p.m. for 10 min to separate aqueous and organic phases, then the upper water layer containing nucleic acid was carefully drawn and transferred into a new 1.5 ml Eppendorf tube. Equal volume of phenol: chloroform: ISO (25:24:1) were added, reverse mixing was done, centrifuged at 10 000 r.p.m. for 10 min and the upper layer liquid was taken and transferred to a new 1.5 ml centrifuge tube. An equal volume of chloroform: isoamyl alcohol (24:1) was added and mixed thoroughly by inversion, centrifuged at 10 000 r.p.m. for 10 min and the supernatant was transferred to a new 1.5 ml Eppendorf tube. Then added 2.5 times of the sample volume of ethanol to precipitate DNA and centrifuged at 12 000 r.p.m. for 10 min after which the ethanol was abondoned. DNA was dried at 55 °C. Proper amount of TE was added to dissolve DNA and then preserved at − 20 °C.

DNA detection of spinal cord scaffold tissue in Wistar rat

Prepare 1% agarose gel. Take 250 ml flask, add 100 ml TBE buffer and 1 g agarose to the buffer and place in a microwave oven, then heat to dissolve it completely. When the solution is transparent, slightly shake and cool to 60 °C. Prepare the gel of 3–5mm thickness. An amount of 1ul sample buffer (6 ×) and 5 ul DNA sample is mixed, then transferred to the gel sample-filling hole. Observe the movement of the band (blue) after the electrophoresis started. When it moves ~ 1 cm to the edge of the plate, stop the electrophoresis. The gel is taken out and placed on the top of the ultraviolet X-ray instrument. Turn on the ultraviolet lamp (360 nm) and observe. Pictures were taken using a software of gel imaging system.

Isolation of rat spinal cord neurons

A Wistar juvenile rat was anesthetized with intraperitoneal injection using 10% chloral hydrate (0.3 ml per 100 g). The state of muscle relaxation and corneal reflex disappearance indicated successful anesthesia. The spinous process and vertebral plate were removed using micro rongeur at T10, and the dura was opened. Anesthetized rats were completely soaked in 75% alcohol solution for 10 min for disinfection, then prone position was taken and fixed in ultraclean table. After skin preparation and regular disinfection, the spinous process and vertebral plate were removed using micro rongeur at T10 and the dura was opened. Carefully wash the blood off the spinal cord tissue. Cut the spinal cord

tissue into small pieces and then transfer into sterile centrifugal tube containing 0.25% EDTA trypsin and gently pipette for 15–20 times. Then the tube was put in the incubator under the condition of 37 °C, 5% CO_2 for 10 min. In the ultraclean table, 2 ml culture medium containing 10% fetal bovine serum was used to suspend the digestion. Tissue homogenate was filtrated with stainless steel filter. The filtrate was collected in the sterile centrifugal tube. The tube was centrifuged at 1200 r.p.m. for 5 min, discard the supernatant, culture medium containing 10% fetal bovine serum was added to the tube, gentlly pipet, and then made into single-cell suspension. The cell concentration was adjusted to 1×10^6 ml^{-1}. The cell suspension was inoculated in cell culture dish, 1 ml in each hole by using 24-hole culture plate, 100 ul in each hole by using 96-hole cell culture plate. Twenty-four hours after culture under the condition of 37 °C, 5% CO_2, medium was changed every other day. Three days after culture, cytosine arabinoside was added into each hole to inhibit the proliferation of non-neuronal cells. The growth condition of the neurons was observed every day.

Identification of rat spinal cord neurons

Coverslip coated with rat tail collagen was put into cell culture dish. Six days after culture, the coverslip was taken out, rinsed with the D-Hanks solution and the polyformaldehyde-DEPC solution was fixed for 20 min. It was washed three times with PBS solution, each for 5 min. The coverslip was treated with 0.3% hydrogen peroxide methanol solution at 37 °C for 30 min to inactivate the endogenous peroxidase. Then it was washed with distilled water three times. Normal goat serum was added for blocking, and then laying for 20 min. The first antibody (Rabbit anti-rat NeuN, neuron-specific enolase (NSE)) with a dilution of 1:200 was added on the coverslip, overnight at 4 °C. It was washed with PBS three times, each for 5 min. The second antibody (biotin Goat anti Rabbit IgG) was added on the coverslip at 37 °C for 30 min. SABC reagent was added, at 37 °C for 30 min, washed with PBS three times, each for 5 min. DAB chromogenic agent was added, 200 ul for each coverslip, at room temperature. Gradient ethanol was used for dehydration, gum was used for sealing the coverslip and then observed under the microscope. For the negative control, PBS was used to replace first antibody, and the other steps were the same.

Growth curve of rat spinal cord neurons

Single-cell suspension was prepared by 0.25% trypsin digestion, and the cell density was adjusted to 5×10^5 ml^{-1} and then seeded onto the 24-hole culture plate. The amount of culture solution was 1 ml for each hole. The cells in three holes were taken out every day for counting to get average value, the counting was repeated for 7 days. The cultured cells which were not used for counting got medium change every other day. The growth curve of the cells was drawn with time as the horizontal axis and cell number as the vertical axis.

Co-culture of spinal cord neurons and acellular spinal cord scaffold *in vitro*

The ASCS was trimmed into small pieces (~0.5 cm × 0.3 cm). The third generation of spinal cord neurons was used in this experiment, and the cell density was adjusted to 1×10^5 ml^{-1}. The cells were transplanted onto the scaffold, which was then put into the culture dish containing the medium of 10% fetal bovine serum. The culture dish was placed in the incubator at 37 °C, 5% CO_2. Then the inverted microscope was used to observe the cell growth.

MTT was used to assay the viability of neurons on the acellular spinal cord scaffold

Exogenous MTT(3-(4,5-dimethylthiazol-2-yl)-2,5-diphenyltetrazolium bromide) was reduced to formazan that precipitates inside the cells by succinate dehydrogenase of mitochondria in living cells. However, the dead cells do not possess this function. Dimethylsulfoxide was then used to dissolve formazan. Microplate reader was used to detect the absorbance value (OD value) at the light wavelength of 490 nm. The more the formazan was produced, the more were the number of living cells. That is to say, the higher the OD value, the more the number of living cells.

Trypsin was used to digest the neurons that were implanted on the ASCS. Then the cell suspension was seeded on the bottom of the culture plate. The well-cultured cells (80–90% fusion) were seeded in 96-well plates (5×10^4 cells per well). After incubation for 24 h, 10 μl MTT solution (5 mg ml^{-1} MTT in PBS, pH 7.4) was added to each well, and the plate was incubated for an additional 4 h. After removing the medium, the wells were washed by PBS, and then the intracellular formazan crystals were extracted into 100 μl dimethylsulfoxide. The absorbance was recorded at 490 nm by a plate reader, and the cell viability relative to the control untreated cells could be calculated from the average value of six parallel wells.

Histological observation

H&E stain. The ASCS of Wistar rat was fixed with 4% polyformaldehyde, water washing, gradient ethanol dehydration for 2 h and xylene for 30 min, and immersed with soft wax at 60 °C for 3 h to make package into paraffin mass. Prepared paraffin mass was cut into serial sections with a thickness of 5 μm; the cut tissue was put on the glass slide treated with polylysine, then baked at 60 °C for 30 min. After cooling to room temperature, xylene was used to dewax, washed with gradient ethanol. Hematoxylin staining was used for 5 min and then flushed by ddH2O, which followed by eosin staining for 2 min. Then, the tissue slide was observed by using conventional microscopy after dehydration and mounting.

Myelin staining

The ASCS of Wistar rat was fixed with 4% polyformaldehyde, water washing, gradient ethanol dehydration for 2 h and xylene for 30 min, and immersed with soft wax at 60 °C for 3 h to make package into paraffin mass. Prepared paraffin mass was cut into serial sections with thickness of 5 μm; the cut tissue was put on the glass slide treated with polylysine, and then baked at 60 °C for 30 min. After cooling to room temperature, xylene was used to dewax, washed with gradient ethanol. The tissue was put into luxol fast blue solution for staining at 60 °C for 2 h, rinsed with 95% ethanol for 1 min, washed with ddH2O for 15 s, wash with 0.05% lithium carbonate solution for 15 s, separated with 70% ethanol for 20 s and washed with ddH2O for 30 s. It was then put into periodate oxidation liquid for 5 min, and washed with ddH2O for 10minl and with schiff agent for 15 min at room temperature. Sulfite washing was done for 6 min, elution with ddH2O was for 15 s, hematoxylin elution was for 3 min followed by washing with ddH2O for 5 min, dehydrating, transparent and mounting and using conventional microscopy to observe.

Scanning electron microscope observation

The ASCS was washed with 0.1 mol l^{-1} Na2HPO4-NaH2PO4 (7.2) buffer for 30 s, repeated three times, then placed into 2.5% glutaraldehyde and 2% polyformaldehyde mixture for fixation for 1.5 h, rinsed with 0.1 mol l^{-1} na2hpo4-nah2po4 (7.2) buffer five times (15 min at each time), 50, 70, 90 and 100% ethanol was used for dehydration, dehydration with 100% ethanol three times (15 min at each time), the sample was then replaced with 100% isoamyl (containing anhydrous CaCl2) three times (10 min at each time). The samples got frozen and dry for 4 h by using freeze-drying instrument, conductive adhesive tape was put on the scanning electron microscope sample stage, the freeze-dried sample was put on the conductive tape with a toothstick and the treated samples were set under the scanning electron microscope, with magnification ascending, and then observed and photographed.

RESULTS

Morphological observation of acellular spinal cord scaffold

The prepared ASCS was milky white, translucent and flat cylindrical. Diameter and length were slightly shorter; it had a soft texture, toughness and no odor (Figure 1a).

Myelin staining

There was no intact myelin components in the ASCS. A few of irregular myelin fragments showed in the scaffold with blue color. The myelin sheath was removed basically. There was no presence of the purple red nucleus, and the cell components were completely removed (Figure 1b).

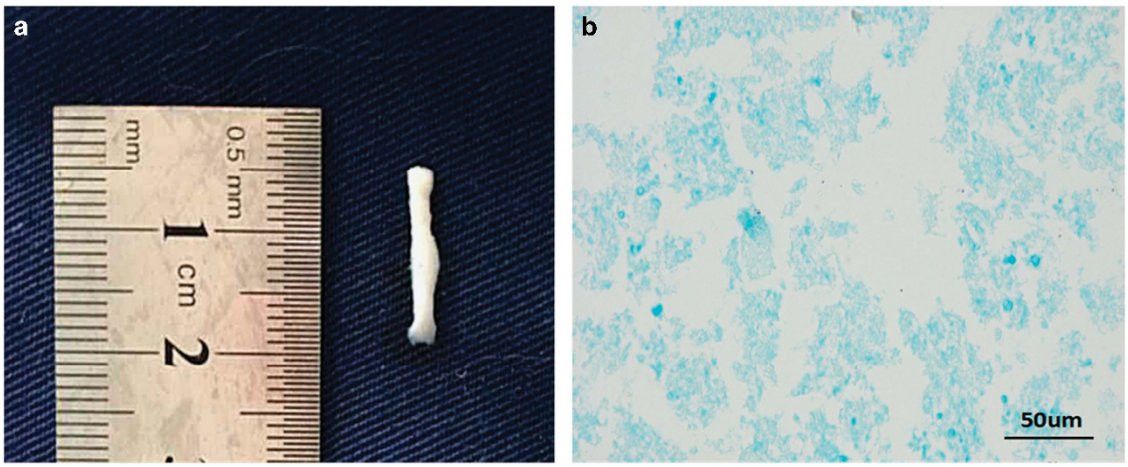

Figure 1 (**a**) Morphological observation of the Wistar rat acellular spinal cord scaffold. The scaffold was milky white, translucent, flat cylindrical, diameter and length were slightly shorter, soft texture, toughness and no odor. (**b**) Luxol fast blue (LFB) staining showed there was no intact myelin components in the prepared acellular spinal cord scaffold. There was no presence of the purple red nucleus, and the cell components were completely removed.

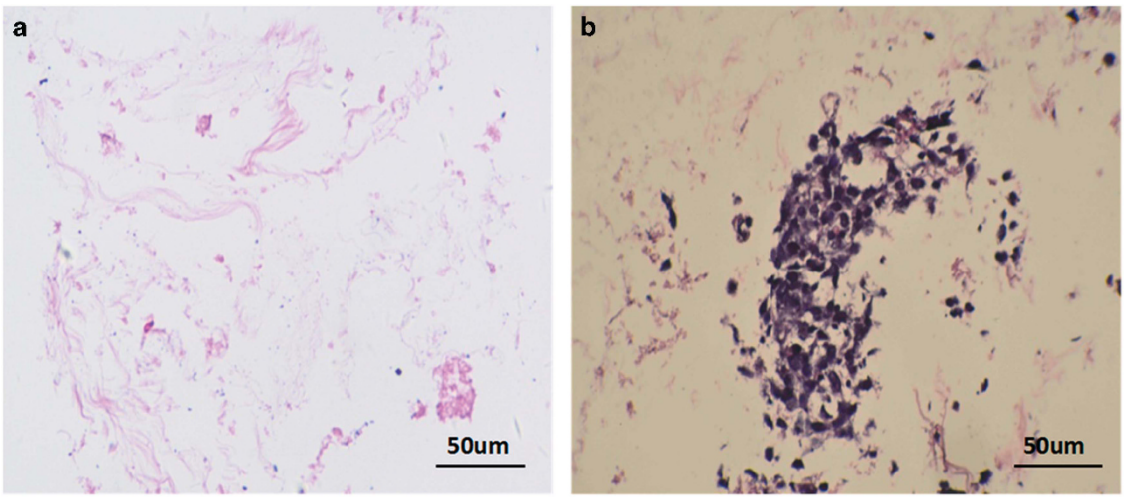

Figure 2 H&E staining morphological observation of the Wistar rat acellular spinal cord scaffold. (**a**) Mesh structure appears on cross section of the ASCS. Cellular components were removed completely. The wall of the mesh hole is composed of extracellular matrix composition with pink staining; there are no cell residues inside and outside the mesh structure. (**b**) After co-culture, the spinal cord neurons adhered to the pore structure of the ASCS, and the cells grew well in the channel of the scaffold to form the region of cell aggregation. H&E, hematoxylin and eosin.

H&E staining

Mesh structure appears on a cross section of the ASCS. Cellular components were removed completely and the nucleus with blue granules and red cytoplasmic stain has not been found. Axons and myelin sheaths were removed. The wall of the mesh hole is composed of ECM composition with pink staining; there are no cell residues inside and outside the mesh structure (Figure 2a).

After hematoxylin and eosin staining of co-culture, the spinal cord neurons adhered to the pore structure of the ASCS, and the cells grew well in the 3D channel of the scaffold to form the region of cell aggregation, which will not influence the spatial structure of the ASCS. This means that there is good biocompatibility and adaptability between the implanted neurons and the scaffold (Figure 2b).

Tissue DNA detection

After the detection of DNA agarose gel electrophoresis, no DNA bands were detected in the prepared ASCS. This means the cell components were completely removed (Figure 3).

Observation of neuron cell morphology and Immunohistochemistry

The spinal cord neuron showed round shape after digestion. Twenty-four hours after being inoculated in the culture plate, the cells were attached to the bottom of the plate and showed irregular shape. Few of the cells that suspend in the medium showed a round shape. Those attached cells grew faster and gradually covered the whole bottom of the plate. The cells showed an irregular shape, and some of them showed fusiform shape (Figure 4a).

NSE staining showed that the cell cytoplasm was stained with brown color, and the nucleus was stained with purple blue. Cell morphology showed irregular shape with a different length of the process. The axons were longer. This means that the prepared cells were spinal cord neurons (Figure 4b).

Results of cell counting

As seen from the results of cell counting, the cell doubling time is ~3–4 days (Table 1).

Neurons cultured from rat spinal cord showed exponential growth; the cell grew faster at 1–4 days after passage. At the fifth day after passage, the cell number reached the maximum. After the fifth day, cell growth entered platform stage. After the seventh day, the cell number began to decline (Figure 5).

Results of immunohistochemistry after co-culture. NSE is highly specifically located in neurons and neuroendocrine cells. After staining of NSE, the cell cytoplasm was stained with brown color, and the nucleus was blue (Figure 6a). NeuN staining mainly combined with DNA of neurons, so the nucleus of neurons was stained with blue color (Figure 6b). As is seen from the results, the implanted cells express the NSE and NeuN antigen, which means the cells growing on the scaffold were neurons. The pore structure of the scaffold was filled with neurons, which showed fine growing state.

Scanning electron microscope observation

The ASCS showed irregular mesh structure, and ECM was arranged layer by layer, which forms irregular circular cavity and excellent 3D network porous structure. The porous structure has thin wall and larger surface area. The holes communicated with each other. No cellular components were found. Axons and myelin sheath structure completely disappeared. Certain roughness appeared on the surface of the ASCS ECM (Figure 7a).

As is seen from the scanning electron microscope observation, the ASCS showed irregular mesh structure and ECM arranged layer by layer, forming irregular circular cavity, which possesses the excellent 3D network porous structure. The implanted cells adhered on the surface of the scaffold; the structure of axons and myelin sheath was visible (Figure 7b).

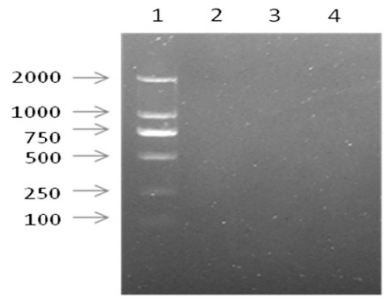

Figure 3 Agarose gel electrophoresis map of DNA (1: Maker; 2–4: the Wistar rat acellular spinal cord scaffold). No DNA bands were detected in the prepared acellular spinal cord scaffold. A full color version of this figure is available at the *Spinal Cord* journal online.

Results of MTT. MTT results showed that there was no significant difference between the cultured neurons on the scaffold and the cells in control group. After calculation, the survival rate of co-cultured cells was (97.53+1.52%).

DISCUSSION

Primary SCI caused by mechanical force can lead to loss of spinal cord tissue. Second injury will cause cell necrosis and accumulation of glial cells, which will finally cause the formation of cavity or glial scar. Without the help of the scaffold to bridge, the remaining axons hardly pass through the injured area to make effective synaptic connection.[35] In this experiment, the ASCS was designed to be used as a bridge to guide the axons to grow, and the neurons implanted on the scaffold were intended to be applied as a relay station to accelerate this process.

Transplanted biomaterials can be used as an effective scaffold for the treatment of SCI. The property of these materials should adapt to the soft nature of the host tissue. However, the nature of most traditional high polymers is rigid, not soft. This will definitely affect their layout and adjustment when being used in the irregular organization. In fact, they may even lead to further compression of the surrounding intact spinal cord tissue.[36,37] Nanomaterials can be adjusted to a variety of different shapes and surfaces when compared

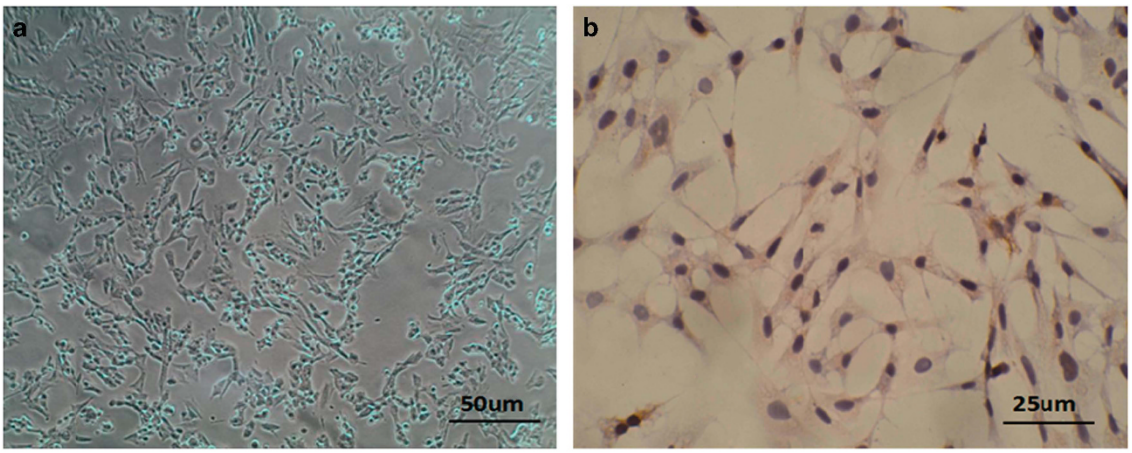

Figure 4 Observation of neuron cell morphology and immunohistochemistry. (**a**) The spinal cord neuron showed round shape after digestion. Twenty-four hours after inoculating in the culture plate, the cells attached to the bottom of the plate and showed irregular shape. (**b**) The cell cytoplasm was stained with brown color and the nucleus was stained with purple blue. Cell morphology showed irregular shape with a different length of the process. The cultured cells expressed the NSE antigen, which means that the prepared cells were spinal cord neurons.

Table 1 Cell counting at different time points

Time	*1 Day*	*2 Days*	*3 Days*	*4 Days*	*5 Days*	*6 Days*	*7 Days*
Cell number ($\times 10^4$)	4.63 ± 0.35	6.56 ± 0.77	8.25 ± 1.26	11.14 ± 0.33	12.85 ± 1.34	11.28 ± 0.84	10.39 ± 0.76

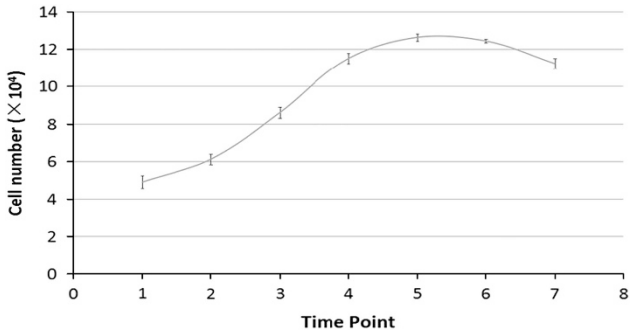

Figure 5 Cell growth curve of rat spinal cord neuron cells. The cell grew faster at 1–4 days after passage. At the fifth day after passage, the cell number reached the maximum. After the fifth day, cell growth entered platform stage. After the seventh day, the cell number began to decline. A full color version of this figure is available at the *Spinal Cord* journal online.

with the micron materials. Especially for the self-assembling fiber scaffold, this scaffold can turn to liquid or soft gel when implanted into the host. Therefore, they can minimize the compression of the adjacent tissue, which is ideal for filling cavities and cracks in the injured spinal cord. However, the immunogenicity limits their application.[36]

In the early stages after SCI, many activated microglia and macrophages migrate to the damaged area to remove the invading microbes and debris of damaged cells.[38] From the third to fifth day after SCI, many of the oligodendroglia precursors, astrocytes and meningocytes also aggregate in the lesion area. These cells are tightly interwoven and secrete a large number of inhibitory factors to finally form glial scar. Because of the physical and chemical barrier, glial scar will produce poor micro-environment for nerve regeneration.[39] Therefore, the implanted scaffold should possess the ability to reduce the inflammatory response and form glial scar to create a better micro-environment for nerve repair promotion. The function of spinal cord

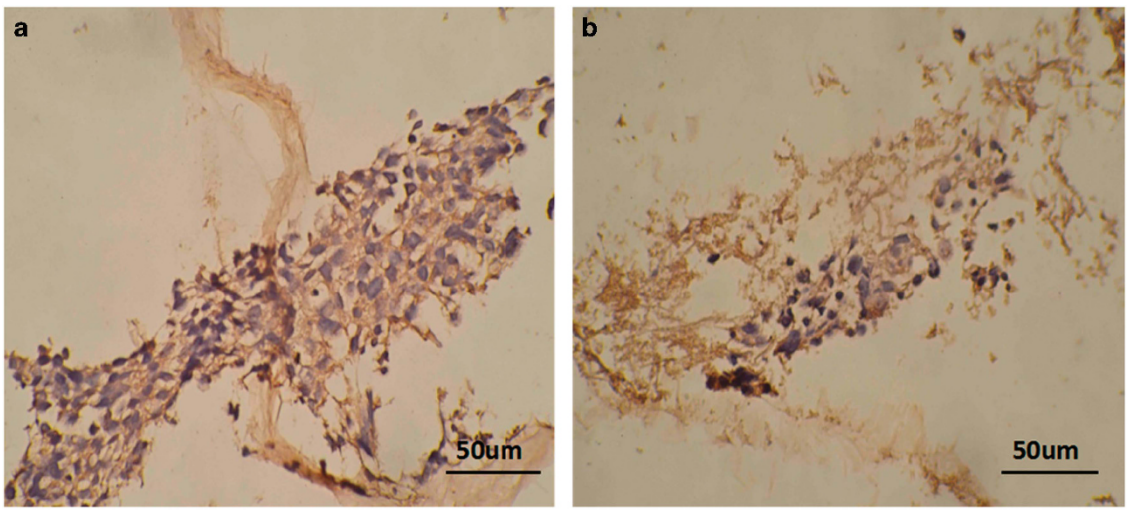

Figure 6 After the cells were co-cultured with ASCS. (**a**) The cells expressed NSE antigen, cell cytoplasm was stained with brown color and the nucleus was blue. (**b**) The cells expressed NeuN antigen. The nucleus of neurons was stained with blue color, which means the cultured cells were neurons.

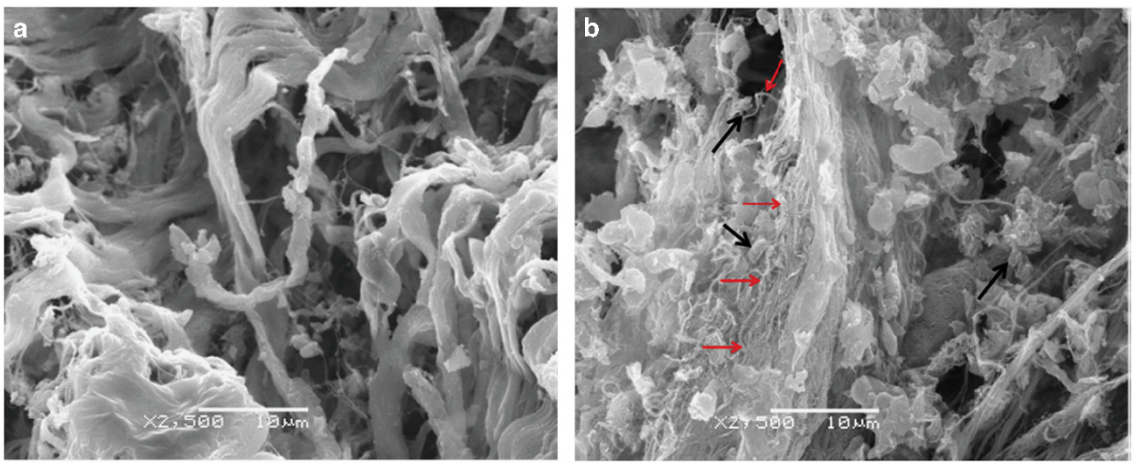

Figure 7 Morphological observation of the Wistar rat acellular spinal cord scaffold observed by scanning electron microscope. (**a**) Before co-culture with neurons, the acellular spinal cord scaffold showed irregular mesh structure, and extracellular matrix was arranged layer by layer, which formed irregular circular cavity and the excellent three-dimensional network porous structure. No cellular components were found on the prepared ASCS. (**b**) After co-culture with neurons, the implanted cells adhered on the surface of the scaffold, the structure of axons and myelin sheath was visible (black arrow showed neuron, red arrow showed axons)

is mainly considered as the transmission station of motor and sensory signals between the brain and the other sense organs of the body. Mechanical stress and secondary damage will lead to axonal degeneration and rupture after SCI. Axonal injury and discontinuity are the main causes of functional defects after SCI.[40,41] Therefore, it is the key step to improve axonal regeneration and synaptic reconstruction. Although some methods have been applied to stimulate axonal regeneration after SCI, axonal regeneration is highly randomized, and regenerated axons do not grow into the damaged tissue. Artificial biomaterials provide support for axonal regeneration as a bridge.[42] Ideal biomaterials for spinal cord repair should meet the following criteria: good biocompatibility, biodegradability, mechanical properties and low neurotoxicity. Guo *et al*[43] implanted acellular rat spinal cord and fresh rat spinal cord into rat paraspinal muscle. The results showed that infiltration of neutrophils and lymphocytes can be found at 1 week post operation in acellular spinal cord graft group, and infiltration of a few lymphocytes at 2 weeks post operation. However, in the fresh spinal cord graft group, there were still infiltration of lots of lymphocytes at 4 weeks post operation, which means ASCS has good biocompatibility.

For axonal regeneration, scaffold biomaterials should also have suitable morphology to guide axonal elongation to pass through the lesion site of spinal cord. Recently, most of the research about tissue engineering is aimed at the modification of biological materials before implantation. Lots of evidence showed, when compared with the traditional biological materials, that nanofiber scaffold has better mechanical and chemical properties to promote axonal regeneration.[44] The experiment of Liu and co-workers showed that,[45] after 24 h of clamp compression injury to the spinal cord tissue, inflammation response and glial scar formation of spinal cord are significantly reduced after local lesion site injection of K2(QL)6 which is a kind of super absorbent polymer. The study of Tysseling-Mattiace *et al* demonstrated that RADA-1 or super absorbent polymer IKVAV has good compatibility with spinal cord; it will also reduce the recruitment of astrocytes/microglia and macrophages after SCI.[46,47] However, it still hard to adjust the microfiber arrangement in the spinal cord. In this experiment, the ASCS can be considered as the most suitable material to transplant, because it has the same microstructure as the spinal cord.

In recent years, multiple types of cells have been used in the treatment after SCI, including embryonic stem cells, induced pluripotent stem cells, neural stem cells, mesenchymal stem cells, olfactory ensheathing cells, Schwann cells and so on. According to the nature of various cell types, transplanted cells can replace lost parenchymal cells and release a variety of bioactive molecules to promote regeneration of the endogenous nerve, reducing secondary damage. The cells can also differentiate into neurons to reweave the neuronal circuits and differentiate into oligodendrocytes to promote myelin formation.[48–50] However, under the most condition of SCI, open cracks or cystic cavities are usually formed in the damage area after SCI. Direct injection of cells into the host tissue will cause accidental injury.[51] In addition, it is difficult for the transplanted cells to survive in the cracks or cavities. One possible approach to solve the problem is to implant the cells onto a scaffold that can be used as a bridging material to fill the cracks and cavities. Optimal tissue engineering is to create a 3D structure that is similar to the natural ECM. The diameter of the fiber should be in the range of 50–500 nm. Traditional technology of artificial biological materials cannot produce fibers with diameters <10 nm. As a matter of fact, the cells in the traditional scaffold are entirely in the form of two-dimensional. Because of this, only one side of the implanted cell is directly exposed to the scaffold, whereas other sides of the cells are exposed to the medium *in vitro* or to the body fluid environment *in vivo*.[52] Therefore, the cells are partially polarized. This kind of environment and condition would lay an adverse effect on implanted cells, such as survival, proliferation, migration and differentiation. In contrast, the 3D nanofiber scaffold can fully accommodate the whole implanted cell. In these scaffolds, a variety of growth factors, cytokines, nutrients and signals can three-dimensionally communicate with the implanted cells, so that the micro-environment is considered to imitate the natural one.[53]

A number of different drug therapies have been used in clinical trials for the treatment of SCI. The effect of these drugs may be expressed in the promotion of neural protection or neural regeneration.[54] However, after SCI, there are still many shortcomings in traditional administration methods for the promotion of nerve protection or nerve regeneration.[55] The most common drug delivery route is oral absorption or intraperitoneal injection. To meet the effective medicine concentration in the target tissue, the drug must be delivered at a very high dose, so that negative effects may happen on other organ tissues. Another approach is by intrathecal injection. This will inevitably increase the risk of unnecessary damage to the rest of the health organs. Taking the above situation into account, it seems that the drug delivery approach is the key point.[56] Recently, the nanofibrous scaffold, including electrospinning and super absorbent polymer nanofiber scaffold in the treatment of SCI as a drug delivery system has been repeatedly reported.[57,58]

In the preparation process, the ASCS preserved the integrity of the 3D spatial structure. This scaffold possessed a lot of properties, such as low immunogenicity, excellent biological compatibility, closest to the real micro-environment and so on, which are conducive to the growth of cell adhesion.[59] In recent years, most of the literature has proved the superiority of natural spinal cord scaffold materials.[60] Schwann cells were seeded on the ASCS the cells were finally in good growth condition and migrated and proliferated along the scaffold channel. The study of Ribatti *et al* showed that the prepared natural acellular material promoted the growth of vascular cells.[61]

In this experiment, the rat's spinal cord neurons and ASCS were co-cultured *in vitro*, the results showed that the neurons grew in good condition in the channel space of the ASCS. Cell axons were intact and also grew in good condition. The spacial structure of the scaffold was intact with cells tightly arranged on it, which means the neurons and the scaffold have good biocompatibility. This scaffold implanted with neurons may be applied to replace the glial scar or cavity and reconstruct synaptic connection after SCI.

CONFLICT OF INTEREST

The authors declare no conflict of interest.

ACKNOWLEDGEMENTS

This work was sponsored by State Key Program of National Natural Science Foundation of China (81330042), Special Program for Sino-Russian Joint Research Sponsored by the Ministry of Science and Technology, China (2014DFR31210), Key Program Sponsored by the Tianjin Science and Technology Committee, China (13RCGFSY19000 14ZCZDSY00044), National Natural Science Foundation of China (81201399) and National Natural Science Foundation of China (81301544).

1 Ban DX, Ning GZ, Feng SQ, Wang Y, Zhou XH, Liu Y *et al*. Combination of activated Schwann cells with bone mesenchymal stem cells: the best cell strategy for repair after spinal cord Injury in rats. *Regen Med* 2011; **6**: 707–720.

2 Ahmadzadeh G, Kouchaki A, Malekian A, Aminorro'aya M, Boroujeni AZ. The process of confrontation with disability in patients with spinal cord injury. *Iran J Nurs Midwifery Res* 2010; **15**: 356–S362.
3 Bobis S, Jarocha D, Majka M. Mesenchymal stem cells: characteristics and clinical applications. *Folia Histochem Cytobiol* 2006; **44**: 215–230.
4 Hu R, Zhou JJ, Luo CX, Lin JK, Wang XR, Li XG *et al.* Glial scar and neuroregeneration: histological, functional, and magnetic resonance imaging analysis in chronic spinal cord injury laboratory investigation. *J Neurosurg Spine* 2010; **13**: 169.
5 Errmann JE, Shah RR, Chan AF, Zheng B. EphA4 deficient mice maintain astroglial-fibrotic scar formation after spinal cord injury. *Exp Neurol* 2010; **223**: 582–598.
6 Fehlings MG, Hawryluk GW. Scarring after spinal cord injury. *J Neurosurg Spine* 2010; **13**: 165–167.
7 Zhilai Z, Hui Z, Yinhai C, Zhong C, Shaoxiong M, Bo Y *et al.* Combination of NEP 1-40 infusion and bone marrow-derived neurospheres transplantation inhibit glial scar formation and promote functional recovery after rat spinal cord injury. *Neurol India* 2011; **59**: 579–585.
8 Göritz C, Dias DO, Tomilin N, Barbacid M, Shupliakov O, Frisén J. A pericyte origin of spinal cord scar tissue. *Science* 2011; **333**: 238–242.
9 Zhang H, Chang M, Hansen CN, Basso DM, Noble-Haeusslein LJ. Role of matrix metalloproteinases and therapeutic benefits of their inhibition in spinal cord injury. *Neurotherapeutics* 2011; **8**: 206–220.
10 Konovalov NA, Nazarenko AG, Asyutin DS, Solenkova AV, Onoprienko RA, Zakirov BA *et al.* Comprehensive assessment of the outcomes of surgical treatment of patients with metastatic spinal cord injuries. *Zh Vopr Neirokhir Im N N Burdenko* 2015; **79**: 34–44.
11 Zhang C, Morozova AY, Abakumov MA, Gubsky IL, Douglas P, Feng S *et al.* Precise delivery into chronic spinal cord injury syringomyelic cysts with magnetic nanoparticles MRI visualization. *Med Sci Monit* 2015; **21**: 3179–3185.
12 Rahimkhani M, Mordadi A, Varmazyar S, Tavakoli A. Evaluation of urinary interleukin-8 levels in patients with spinal cord injury. *Recent Pat Antiinfect Drug Discov* 2014; **9**: 144–149.
13 Goriely A, Geers MG, Holzapfel GA, Jayamohan J, Jérusalem A, Sivaloganathan S *et al.* Mechanics of the brain: perspectives, challenges, and opportunities. *Biomech Model Mechanobiol* 2015; **14**: 931–965.
14 Tilley DM, Vallejo R, Kelley CA, Benyamin R, Cedeño DL. A continuous spinal cord stimulation model attenuates pain-related behavior *in vivo* following induction of a peripheral nerve injury. *Neuromodulation* 2015; **18**: 171–176.
15 Dalbayrak S, Yaman O, Yilmaz M, Naderi S. Results of the transsternal approach to cervicothoracic junction lesions. *Turk Neurosurg* 2014; **24**: 720–725.
16 Lin E, Long H, Li G, Lei W. Does diffusion tensor data reflect pathological changes in the spinal cord with chronicinjury. *Neural Regen Res* 2013; **8**: 3382–3390.
17 Yang H, Lu X, Wang X, Chen D, Yuan W, Yang L *et al.* A new method to determine whether ossified posterior longitudinal ligament can be resected completely and safely: spinal canal 'Rule of Nine' on axial computed tomography. *Eur Spine J* 2015; **24**: 1673–1680.
18 Dlouhy BJ, Awe O, Rao RC, Kirby PA, Hitchon PW. Autograft-derived spinal cord mass following olfactory mucosal cell transplantation in aspinal cord injury patient: case report. *J Neurosurg Spine* 2014; **21**: 618–622.
19 Hellal F, Hurtado A, Ruschel J, Flynn KC, Laskowski CJ, Umlauf M *et al.* Microtubule stabilization reduces scarring and causes axon regeneration after spinal cord injury. *Science* 2011; **331**: 928–931.
20 Zhang SX, Geddes JW, Owens JL, Holmberg EG. X-irradiation reduces lesion scarring at the contusion site of adult rat spinal cord. *Histol Histopathol* 2005; **20**: 519–530.
21 Ridet JL, Pencalet P, Belcram M, Giraudeau B, Chastang C, Philippon J *et al.* Effects of spinal cord X-irradiation on the recovery of paraplegic rats. *Exp Neurol* 2000; **161**: 1–14.
22 Dolmans DE, Fukumura D, Jain RK. Photodynamic therapy for cancer. *Nat Rev Cancer* 2003; **3**: 380–387.
23 Coupienne I, Bontems S, Dewaele M, Rubio N, Habraken Y, Fulda S *et al.* NF-kappaB inhibition improves the sensitivity of human glioblastoma cells to 5-aminolevulinic acid-based photodynamic therapy. *Biochem Pharmacol* 2011; **81**: 606–616.
24 Jeremic G, Brandt MG, Jordan K, Doyle PC, Yu E, Moore CC. Using photodynamic therapy as a neoadjuvant treatment in the surgical excision of nonmelanotic skin cancers: prospective study. *J Otolaryngol Head Neck Surg* 2011; **40**: S82–S89.
25 Usuda J, Ichinose S, Ishizumi T, Hayashi H, Ohtani K, Maehara S *et al.* Outcome of photodynamic therapy using NPe6 for bronchogenic carcinomas in central airways >1.0 cm in diameter. *Clin Cancer Res* 2010; **16**: 2198–2204.
26 Odergren A, Algvere PV, Seregard S, Libert C, Kvanta A. Vision-related function after low-dose transpupillary thermotherapy versus photodynamic therapy for neovascular age-related macular degeneration. *Acta Ophthalmol* 2010; **88**: 426–430.
27 Kuningas K, Päkkilä H, Ukonaho T, Rantanen T, Lövgren T, Soukka T. Upconversion fluorescence enables homogeneous immunoassay in whole blood. *Clin Chem* 2007; **53**: 145–146.
28 van De Rijke F, Zijlmans H, Li S, Vail T, Raap AK, Niedbala RS *et al.* Up-converting phosphor reporters for nucleic acid microarrays. *Nat Biotechnol* 2001; **19**: 273–276.
29 Chatterjee DK, Fong LS, Zhang Y. Nanoparticles in photodynamic therapy: an emerging paradigm. *Adv Drug Deliv Rev* 2008; **60**: 1627–1637.
30 Abdul Jalil R, Zhang Y. Biocompatibility of silica coated NaYF(4) upconversion fluorescent nanocrystals. *Biomaterials* 2008; **29**: 4122–4128.
31 Idris NM, Li Z, Ye L, Sim EK, Mahendran R, Ho PC *et al.* Tracking transplanted cells in live animal using upconversion fluorescent nanoparticles. *Biomaterials* 2009; **30**: 5104–5113.
32 Chen GY, Liu Y, Zhang YG, Somesfalean G, Zhang ZG, Sun Q *et al.* Bright white upconversion luminescence in rare-earth-ion-doped Y2O3 nanocrystals. *Phys Lett* 2007; **91**: 133–134.
33 Nyk M, Kumar R, Ohulchanskyy TY, Bergey EJ, Prasad PN. High contrast *in vitro* and *in vivo* photoluminescence bioimaging using near infrared to near infrared up-conversion in Tm3+ and Yb3+ doped fluoride nanophosphors. *Nano Lett* 2008; **8**: 3834–3838.
34 Xiong L, Yang T, Yang Y, Xu C, Li F. Long-term *in vivo* biodistribution imaging and toxicity of polyacrylic acid-coated upconversion nanophosphors. *Biomaterials* 2010; **31**: 7078–7085.
35 Neupane J, Ghimire S, Shakya S, Chaudhary L, Shrivastava VP. Effect of light emitting diodes in the photodynamic therapy of rheumatoid arthritis. *Photodiagnosis Photodyn Ther* 2010; **7**: 44–49.
36 Zhang P, Steelant W, Kumar M, Scholfield M. Versatile photosensitizers for photodynamic therapy at infrared excitation. *J Am Chem Soc* 2007; **129**: 4526–4527.
37 Zijlmans HJ, Bonnet J, Burton J, Kardos K, Vail T, Niedbala RS *et al.* Detection of cell and tissue surface antigens using up-converting phosphors: a new reporter technology. *Anal Biochem* 1999; **267**: 30–36.
38 Voura EB, Jaiswal JK. Tracking metastatic tumor cell extravasation with quantum dot nanocrystals and fluorescence emission scanning microscopy. *Nat Med* 2004; **10**: 993–998.
39 Zhang QB, Song K, Zhao JW, Kong X, Sun Y, Liu X *et al.* Hexanedioic acid mediated surface-ligand-exchange process for transferring NaYF4: Yb/Er(or Yb/Tm) up-converting nanoparticles from hydrophobic to hydrophilic. *J Colloid Interface Sci* 2009; **336**: 171–175.
40 Zhang P, Steelant W, Kumar M, Scholfield M. Versatile photosensitizers for photodynamic therapy at infrared excitation. *J Am Chem Soc* 2007; **129**: 4526–4527.
41 Yu MX, Li FY, Chen ZG, Hu H, Zhan C, Yang H *et al.* Laser scanning up-conversion luminescence microscopy for imaging cells labeled with rare-earth nanophospors. *Anal Chem* 2009; **81**: 930–935.
42 Chen ZG, Chen HL, Hu H, Yu M, Li F, Zhang Q *et al.* Versatile synthesis strategy for carboxylic acid functionalized upconverting nanophosphors as biological labels. *J Am Chem Soc* 2008; **130**: 3023–3029.
43 Wang F, Banerjee D, Liu YS, Chen X, Liu X. Upconversion nanoparticles in biological labeling, imaging, and therapy. *Analyst* 2010; **135**: 1839–1854.
44 Li ZQ, Zhang Y. An efficient and user-friendly method for the synthesis of hexagonal-phase NaYF4: Yb, Er/Tm nanocrystals with controllable shape and upconversion fuorescence. *Nanotechnology* 2008; **19**: 345606.
45 Wang M, Mi CC, Liu JL *et al.* One-step synthesis and characterization of water-soluble NaYF4: Yb, Er/polymer nanoparticles with efficient up-conversion fuorescence. *J Alloys Compounds* 2009; **485**: 24–27.
46 Budijono SJ, Shan JN, Yao N, Miura Y, Hoye T, Austin RH *et al.* Synthesis of stable block-copolymer-protected NaYF4: Yb3+, Er3+ up-converting phosphor nanoparticles. *Chem Mater* 2010; **22**: 311–318.
47 Chen GY, Ohulchanskyy TY, Kumar R, Agren H, Prasad PN. Ultrasmall monodisperse NaYF4: Yb3+/Tm3+ nanocrystals with enhanced near-infrared to near-infraredupconversion photoluminescence. *ACS Nano* 2010; **4**: 3163–3168.
48 Wang M, Mi CC, Wang WX, Liu CH, Wu YF, Xu ZR *et al.* Immunolabelling and NIR-excited fluorescent imaging of HeLa cells by using NaYF4: Yb, Er upconversion nanoparticles. *ACS Nano* 2009; **3**: 1580–1586.
49 Audet N, Charfi I, Mnie-Filali O, Amraei M, Chabot-Dore AJ, Millecamps M. Differential association of receptor-G betagamma complexes with beta-arrestin2 determines recycling bias and potential for tolerance of delta opioid receptor agonists. *J Neurosci* 2012; **32**: 4827–4840.
50 Clarke LE, Barres BA. Emerging roles of astrocytes in neural circuit development. *Nat Rev Neurosci* 2013; **14**: 311–321.
51 Colantuoni C, Jeon OH, Hyder K, Chenchik A, Khimani AH, Narayanan V *et al.* Gene expression profiling in postmortem Rett syndrome brain: differential gene expression and patient classification. *Neurobiol Dis* 2001; **8**: 847–865.
52 Colombo JA. Interlaminar astroglial processes in the cerebral cortex of adult monkeys but not of adult rats. *Acta Anat (Basel)* 1996; **155**: 57–62.
53 Figueiredo M, Lane S, Tang F, Liu BH, Hewinson J, Marina N *et al.* Optogenetic experimentation on astrocytes. *Exp Physiol* 2011; **96**: 40–50.
54 Freeman MR, Rowitch DH. Evolving concepts of gliogenesis: a look way back and ahead to the next 25 years. *Neuron* 2013; **80**: 613–623.
55 Freund TF, Katona I, Piomelli D. Role of endogenous cannabinoids in synaptic signaling. *Physiol Rev* 2003; **83**: 1017–1066.
56 Han X, Chen M, Wang F, Windrem M, Wang S, Shanz S *et al.* . Forebrain engraftment by human glial progenitor cells enhances synaptic plasticity and learning in adult mice. *Cell Stem Cell* 2013; **12**: 342–353.
57 Henneberger C, Papouin T, Oliet SH, Rusakov DA. Long-term potentiation depends on release of D-serine from astrocytes. *Nature* 2010; **463**: 232–236.
58 Lee Y, Su M, Messing A, Brenner M. Astrocyte heterogeneity revealed by expression of a GFAP-LacZ transgene. *Glia* 2006; **53**: 677–687.
59 Matyash V, Kettenmann H. Heterogeneity in astrocyte morphology and physiology. *Brain Res Rev* 2010; **63**: 2–10.
60 Nedergaard M, Verkhratsky A. Artifact versus reality: how astrocytes contribute to synaptic events. *Glia* 2012; **60**: 1013–1023.
61 Ross K, Cherpelis B, Lien M, Fenske N. Spotlighting the role of photodynamic therapy in cutaneous malignancy: an update and expansion. *Dermatol Surg* 2013; **39**: 1733–1744.